

Field-cycled PEDRI imaging of free radicals with detection at 450 mT

David J. Lurie, Gareth R. Davies, Margaret A. Foster and James M.S. Hutchison

Department of Bio-Medical Physics and Bio-Engineering,

University of Aberdeen,

Foresterhill,

Aberdeen AB25 2ZD

UK

Corresponding author: Prof. D.J. Lurie
Tel: +44 1224 554061
Fax: +44 1224 685645
email: lurie@abdn.ac.uk

Abstract

This paper describes the design, construction and use of a field-cycled-proton electron double-resonance imaging (FC-PEDRI) system for the detection and imaging of free radicals. The unique feature of this imager is its use of a 450 mT detection magnetic field, in order to achieve good image quality and sensitivity. The detection magnetic field is provided by a superconducting magnet, giving high stability and homogeneity. Field-cycling is implemented by switching on and off the current in an internal, coaxial, resistive secondary magnet which partially cancels the superconducting magnet's field at the sample; the secondary magnet is actively shielded to avoid eddy currents. EPR irradiation takes place at ~5 mT, following which the field is switched to 450 mT in 40 ms for NMR signal detection. Full details of the imager's subsystems are given, and experiments to image the distribution of stable free radical contrast agents in phantoms and in anaesthetised rats are described.

Keywords: PEDRI, field-cycling, Overhauser imaging, free radical

1. Introduction

The Overhauser effect has been employed as a method for imaging and detecting free radicals in biological and other liquid-like samples for more than 15 years. In the method known as Proton-Electron Double-Resonance Imaging (PEDRI) an EPR line of the free radical of interest is irradiated during the acquisition of an MR image, and the NMR signal in regions containing free radicals is modulated by the Overhauser transfer of polarization from unpaired electron spins to water proton spins [1,2]. Provided the free radical concentration is sufficiently high, images collected with and without EPR irradiation will exhibit different intensities in parts of the sample that contain free radicals, and subtraction of the image data sets will yield a “pure” free radical image, showing only regions where free radicals are present.

Field-cycled PEDRI (FC-PEDRI) was introduced in order to counter problems associated with high non-resonant absorption of RF power from the EPR irradiation: in this technique the magnetic field B_0 is switched between low and high levels during the pulse sequence, with EPR irradiation occurring at a low value of B_0 (called the evolution field, B_0^E) and NMR signal detection at a higher value (called the detection field, B_0^D) [2,3]. Since the EPR irradiation is applied at low field (~4 mT) its frequency is also relatively low (~100 MHz) and so the specific absorption rate (SAR) may be reduced to acceptable levels while maintaining the necessary Overhauser enhancement. Detecting the NMR signals at a higher field means that the inherent signal to noise ratio (SNR) remains good, despite the time spent at very low field during the pulse sequence. Figure 1 shows a typical FC-PEDRI pulse sequence.

Previous work has shown that, where there is an upper limit on the acceptable SAR in an FC-PEDRI experiment (for example in animal studies), there is an optimum value of B_0^E of around 5 mT, depending on the EPR linewidth of the free radical and on the maximum permitted EPR irradiation

power [4]. It is also clear from that work, and from earlier work on field-cycling NMR relaxometry [5], that optimization of the SNR, and hence the sensitivity, will be achieved by using as high a detection magnetic field as is feasible. We previously constructed and used a large-sample FC-PEDRI imager with a detection magnetic field of 59 mT [6]. In this paper we describe a new instrument for FC-PEDRI, with a detection magnetic field of 450 mT, and present initial results obtained using the instrument.

2. 450 mT FC-PEDRI Instrument

Figure 2 shows a block diagram of the 450 mT FC-PEDRI system. Many of the constituent modules are commercially available, while others were constructed in-house. The main sub-systems will now be described.

2.1 Field-cycling magnet and power supply

The core of the FC-PEDRI system is the field-cycling magnet. The magnetic field must be sufficiently homogeneous and stable during the detection period of the pulse sequence in order to detect NMR signals and to use them to produce artefact-free images. The desired specification was that the detection field should have homogeneity (after shimming) better than ± 1 ppm over a 60 mm diameter spherical volume (DSV), should stabilise to better than ± 1 ppm of 450 mT within 10 ms after a field ramp from B_0^E to B_0^D and should then be stable within ± 1 ppm during the detection period, to avoid blurring in the readout direction. Furthermore, the reproducibility of the detection field from acquisition to acquisition should be within ± 1 part in 10^8 , in order to avoid ghost artefacts in the phase-encode direction. During the evolution period the magnetic field requirements are less stringent, but the field must be sufficiently homogeneous and stable to allow irradiation of the EPR line(s) of the

free radical under study. Here it was assumed that the narrowest EPR linewidth encountered would be that of the triaryl-methyl (TAM) stable free radical developed by Nycomed [7], so that the shimmed homogeneity during the evolution period should be better than $\pm 10 \mu\text{T}$ over a 60 mm DSV at a typical B_0^E value of 4 mT. To ensure constant efficiency over the duration of each EPR irradiation, the magnetic field should be stable within $\pm 5 \mu\text{T}$ during the evolution period, and the set value of B_0^E should be reproducible from line to line of the pulse sequence within the same tolerance.

In a similar manner to that used in our 59 mT FC-PEDRI instrument [6], the new system employs the field-compensation method of field-cycling [5], in which a primary magnet generates the detection magnetic field with high homogeneity and high stability and a secondary magnet, with lower homogeneity, is used to partially cancel the primary field during the evolution period of the pulse sequence.

The primary magnet, which generates the 450 mT detection field, is a conventional, self-shielded, superconducting whole-body MRI magnet (Oxford Magnet Technology, Oxford, UK) with internal bore 830 mm, originally designed to operate at up to 500 mT. As discussed above, the homogeneity and stability requirements of the “field-offset” secondary magnet are less stringent than for the primary magnet, so that a relatively simple, low-inductance coil can be used, making it possible to switch the current rapidly, without having to employ an inordinately high drive voltage. On the other hand, the field-offset coil must be actively shielded in order to avoid eddy currents in the primary magnet coil, and this does add to the total inductance of the offset coil assembly. However, the main advantage of the field-compensation approach is the relative ease of maintaining field stability during the detection period. The current in the secondary magnet must simply be held at zero, leaving the stable field from the primary magnet. A steady zero current is much easier to control than is a non-zero current, as would be required in a single-coil magnet design (where the current required to produce the detection field could well be several hundred amperes).

An actively-shielded, resistive field-offset secondary magnet coil was designed and built to the above specification by Tesla Engineering Ltd. (West Sussex, UK). The coil assembly also incorporates an integrated shim and gradient coil set (see section 2.2 below). The internal diameter of the complete coil assembly is 120 mm and its outer diameter is 752 mm. The important electrical characteristics of the combined field-offset/active shield coil are as follows: DC resistance 140 m Ω , inductance 5 mH, field strength per unit current 0.511 mT/A. The current required to completely offset the primary magnet's field of 450 mT is therefore 880 A, at which the dissipation in the coil assembly is 108 kW. The system is designed to operate at a maximum duty cycle of 66%, with an average dissipation of 73 kW; this heat is removed from the coil assembly by a closed-circuit water-cooling system together with a high-capacity chiller unit (Thermo-Neslab, Inc., NH, USA, model HX-2000).

Figure 3 shows a schematic diagram of the complete magnet system, comprising the superconducting magnet, field-offset coil with its active shield coil, gradient and shim coils. Figure 4 shows a photograph of the complete magnet system with all its coils installed.

Magnetic field cycling is accomplished by altering the current driven through the actively-shielded field-offset coil, via an analog control signal generated by the pulse sequence controller (see section 2.3 below). The field-offset coil's power supply is comprised of four power-supply amplifiers connected in parallel (Copley Controls Inc., MA, USA, model 266), themselves powered by six 15 kW DC power supplies operating in parallel (Electronic Measurements, Inc., NJ, USA, model ESS 601). In order to meet the stringent field-stability requirements (see above) the Copley power-supply amplifier subsystem includes a feedback loop which incorporates a high-precision zero-flux current transducer and control unit (Danfysik A/S, Jyllinge, Denmark, model Ultrastab 860R). This enables continuous monitoring of the current driven through the field-offset and active-shield coils, with automatic correction to account for any drift in the gain of the power-supply amplifier.

To achieve the maximum possible Overhauser enhancement it is necessary to irradiate the free radical's EPR for at least $3 \cdot T_1$. In order to accommodate long- T_1 samples in *in vitro* experiments, it was desirable to have the capability of EPR irradiation periods as long as 2000 ms. Following the EPR irradiation it is necessary to ramp up the magnetic field from the evolution value (~ 4 mT) to the detection field (450 mT) in a time that is short compared to the sample's T_1 . The Copley power supply amplifier system is able to ramp the magnetic field at the sample from the evolution value to 450 mT (or *vice versa*) in 40 ms.

2.2 Gradient and shim coils and power supplies

Magnetic field gradient coils (X, Y, Z) and shim coils (Z^2 , Z^3 , Z^4 , XY, Z^2-Y^2 , ZX, ZY and B_0) were integrated into the structure of the field-offset and active-shield coil set described above (Tesla Engineering Ltd.). The gradient coils were designed to achieve pulsed magnetic field gradients up to 60 mT/m. They were driven by standard gradient amplifier power supplies, operating in current-control mode (Techron, Inc., IN, USA, model 8522) which easily accommodated the 0.5 ms gradient switching times typically used in the FC-PEDRI pulse sequences.

In order to achieve the necessary magnetic field homogeneity during both the evolution and detection periods of the field-cycling pulse sequence, it was necessary to be able to switch between “evolution-field” and “detection-field” shim settings under control of the pulse sequence. A special shim power supply was obtained for this purpose (Resonance Research, Inc., MA, USA). Both sets of shim settings are downloaded to the power supply prior to the initiation of a pulse sequence, and it is then possible to switch between the two sets during operation of the pulse sequence via a single “shim-switch” TTL logic line from the pulse sequence controller.

2.3 Pulse sequence controller

The system is controlled by a commercially-available console (Tecmag, Inc., TX, USA, model Apollo). This controls all functions of the imager through software running on a separate PC, which is connected to the console unit via a proprietary interface card. The pulse sequence controller also includes a separate digital-to-analog (DAC) module to provide the X, Y and Z gradient-driver voltage waveforms. The DAC module is connected to the console by three separate “RJ45” networking (Ethernet) cables (one for each of the gradients), while the output waveforms (between -10 V and $+10$ V) are fed to the appropriate gradient amplifiers by screened twin-cored coaxial cables.

In order to control the magnetic field during the FC-PEDRI pulse sequence it is necessary for the pulse sequence controller to generate a fourth high-precision, high-stability analog output, in addition to the usual three gradient waveforms. This was achieved by generating a waveform table during the pulse sequence, and sending the 16-bit data to the console’s parallel output port in order to drive a separate, home-built DAC module, the output of which was connected to the input of the field-offset coil’s power-supply amplifier (see above). The DAC module was based on a high-precision DAC chip (Analog Devices AD669), and also employed a precision voltage reference (National Semiconductor LM169). The DAC module was located within the rack of the power supply amplifier, and its low voltage supply was derived from that unit. In this way the connection (over a distance of about 5 metres) between the console and the power-supply amplifier sub-system was entirely digital, thus avoiding unwanted pick-up from the cables taking the power supply amplifier’s output (up to 880 A) to the field-offset coil. In order to further minimise the possibility of interference, the parallel input of the DAC chip was opto-isolated within the module.

The pulse sequence controller also has the facility to output a number of TTL logic signals during the pulse sequence, in order to control external modules such as the shim power supply (toggling

between its evolution and detection field shim settings, see above) and enabling/disabling RF power amplifiers (see below).

2.4 RF system

The console provides separate RF outputs for the NMR transmit channel (19.15 MHz) and the EPR transmit channel (between 90 MHz and 110 MHz), each with timing and amplitude controlled from the pulse program. NMR excitation pulses are sent to a power amplifier (Analogic Corporation, MA, USA, model AN8061), then through a home-built, passive transmit/receive (T/R) switch to the RF coil. NMR signals pass from the RF coil through the T/R switch and are pre-amplified by another home-built unit before passing to the console's RF input for further amplification, demodulation and processing. EPR irradiation signals generated by the console are amplified by a power amplifier (Amplifier Research, PA, USA, model 75AP250) before being sent to the EPR resonator through a power meter (RS Components, UK, model W570), which allows the forward and reflected RF power to be monitored.

Two different NMR/EPR RF coil/resonator assemblies were constructed for use with the imager. Both were designed for imaging samples up to 5 cm diameter, including live animals (typically rats, up to ~200 g body weight). The first used an Alderman-Grant resonator [8] to transmit the linearly-polarized EPR irradiation at 93 MHz, together with a separate, coaxial, saddle-coil for NMR transmission and reception at 19.15 MHz, also in a linearly-polarized fashion. The second assembly used a double-resonance birdcage resonator to perform EPR irradiation at 106 MHz as well as NMR transmission and reception. In this case, all three modes were circularly polarized, with the intention of optimising SNR and minimising SAR.

In the double-coil assembly, an Alderman-Grant resonator (75 mm diameter, 145 mm length) is supported inside a 115 mm diameter cylindrical RF shield of 260 mm length. The resonator is capacitively coupled through a trimmer capacitor which allows the matching to be adjusted. The NMR saddle coil is 50 mm in diameter and 65 mm in length and is mounted co-axially inside the Alderman-Grant resonator. Again, a trimmer capacitor provides matching adjustment of the RF coil. Unloaded quality factors (Q-factors) of the assembled coil/resonator were measured as 280 for the NMR saddle coil and 580 for the Alderman-Grant resonator used for EPR irradiation.

The true double-resonance coil assembly is a low pass, eight-leg, birdcage resonator supporting quadrature modes at both frequencies. It was designed following the work of Shen *et al.* [9]. The resonator is 60 mm in diameter and 80 mm long and is supported inside a 120 mm diameter cylindrical RF shield. For each frequency two inductive coupling loops are used to drive two modes of resonance in which the linearly-polarized RF magnetic fields are perpendicular to the axis of the resonator and to each other; driving these modes in quadrature produces a circularly-polarized RF magnetic field. For the two proton frequency modes, coaxial cables link the coupling loops to two ports of a home-built quadrature hybrid junction. During NMR transmission this introduces a $\pi/2$ phase difference to the RF being fed from the transmitter, while for NMR signal reception it removes the $\pi/2$ phase difference from the signals coming back from the resonator, as well as isolating the transmitter from the pre-amplifier. The EPR irradiation signal from the EPR amplifier is connected to the other two ports of the resonator via another hybrid junction, to generate the circularly polarized RF field at the EPR frequency. Unloaded quality factors of 80 (NMR) and 160 (EPR) were measured.

Although the true double-resonance birdcage resonator represented a more elegant approach than the Alderman-Grant/saddle coil assembly, it can be seen that the Q-factors of both the NMR and EPR modes were considerably lower in the case of the former design – for example, 80 (birdcage) *versus* 280 (saddle) in the case of the NMR structures – probably due to the considerable complexity of the

quadrature double-resonance birdcage resonator. This meant that it was the Alderman-Grant/saddle coil assembly that delivered the superior performance, in terms of SNR, sensitivity and EPR irradiation efficiency. The only disadvantage of that assembly was that its internal diameter was smaller (50 mm as opposed to the birdcage's 60 mm) due to the necessity to have coaxial structures with space between them.

3. Use of the imager

3.1 Phantom studies

In order to test the system, a phantom was constructed using glass tubes (8 mm internal diameter) containing a range of concentrations of TEMPOL nitroxide free radical (4-hydroxy-2,2,6,6-tetramethylpiperidine-1-oxyl, Sigma/Aldrich, Poole, UK) in aqueous solution. Figure 5 shows field-cycled images of the phantom obtained with and without EPR irradiation, together with a “Difference” image obtained following subtraction of the complex with- and without-EPR data sets. It can be seen that the images are artefact-free. In particular, there is no evidence of ghosting in the phase-encode (vertical) direction, despite the very large difference between B_0^E and B_0^D (4.6 mT and 450 mT respectively) – this indicates sufficiently good reproducibility and stability of the detection field, due to the correct operation of the actively-shielded field-offset coil. Further evidence of the lack of eddy-currents associated with field-switching is provided by the absence of “smearing” in the readout (horizontal) direction, which might have arisen had there been magnetic field instability during the signal sampling window.

3.2 *In vivo* studies

Locally-bred male Sprague Dawley rats, body weight (BW) ≈ 175 g were used for *in vivo* studies. The animals were anesthetized by using a single intraperitoneal dose of a ketamine/xylazine mixture (41 mg/kg BW ketamine (Vetalar, Parke-Davis, Pontypool, UK) and 20.5 mg/kg BW xylazine (Rompun, Bayer, Bury St Edmunds, UK). A polythene cannula (0.96 mm outer diameter) was surgically inserted into the left external jugular vein. After placing the animal supine within the FC-PEDRI system, a dose of free radical contrast agent was given via the cannula. In some experiments, the free radical used was 3-carboxy-proxyl (Sigma-Aldrich, Poole, UK). In the work presented here the narrow-line contrast agent triaryl-methyl (TAM, variant OX063) was used [7], which was obtained as a gift from Nycomed-Amersham, Malmö, Sweden. Solid TAM was dissolved to a concentration of 200 mM in phosphate-buffered physiological saline. The pH of the injection solution was close to neutral. A dose of 0.58 mmol/kg was administered by injecting 0.5 ml via the cannula, over the course of 45 s. At the end of the experimental period, animals were killed, under anesthetic, by an overdose of sodium pentobarbitone. All animal procedures were carried out in accordance with local guidelines and under British Home Office Project Licence No. PPL 60/3177 (MAF).

Figure 6 shows a set of coronal FC-PEDRI images (EPR-on, EPR-off and Difference) of a 172 gram rat, 51 minutes after injection of a dose of TAM; imaging parameters are listed in the figure caption. A slice thickness of 30 mm was used, in order to visualize the free radical independent of its anterior-posterior position within the animal. In the difference image the animal's kidneys and bladder can clearly be seen. The ureters are also clearly visible, despite the fact that they represent only a small fraction of the volume of a voxel (the voxel dimensions are $30 \times 0.8 \times 0.8$ mm).

4. Conclusions

We have built a field-cycled PEDRI imager with a detection magnetic field of 450 mT, suitable for detecting and imaging free radicals in biological samples and small animals up to 5 cm in diameter.

The relatively high detection field allows an improvement in spatial resolution and image quality relative to our earlier FC-PEDRI imager, which used a detection field of 59 mT [6]. A further advantage of the new system is its ability to produce conventional (i.e. non-field-cycled) images at a fixed field of 450 mT; these high-resolution images are advantageous in positioning samples prior to study by FC-PEDRI. As well as its use in the study of biological and *in vivo* samples, the new FC-PEDRI system is expected to be invaluable for the investigation of free radical contrast agents in non-biological samples, for example in environmental science applications [10].

Acknowledgements

Funding was provided by the Engineering and Physical Sciences Research Council under grant number GR/M46488/01 and by the University of Aberdeen. The authors thank Mr. Takuya Yokoyama for writing software to facilitate subtraction of complex data sets, Mr. Eddie Stevenson for help with the mechanical construction of the FC-PEDRI system and Dr. Klaes Golman of Nycomed-Amersham for the kind gift of TAM radical.

References

1. Lurie DJ, Bussell DM, Bell LH, Mallard JR. Proton-electron double magnetic resonance imaging of free radical solutions. *J.Magn.Reson.* 1988;76:366-370.
2. Lurie DJ. Proton-electron double-resonance imaging (PEDRI). In: L.J. Berliner, editor. *In Vivo EPR (ESR): Theory and Applications*. New York: Kluwer Academic / Plenum Publishers; 2003. p 547-578.
3. Lurie DJ, Hutchison JMS, Bell LH, Nicholson I, Bussell DM, Mallard JR. Field-cycled proton electron double-resonance imaging of free radicals in large aqueous samples. *J.Magn.Reson.* 1989;84:431-437.
4. Youngde W, Planinsic G, Lurie DJ. Optimization of field-cycled PEDRI for in vivo imaging of free radicals. *Phys.Med.Biol.* 2001;46:2531-2544.
5. Noack F. NMR field-cycling spectroscopy - principles and applications. *Progr. NMR Spectrosc.* 1986;18:171-276.
6. Lurie DJ, Foster MA, Yeung D, Hutchison JMS. Design, construction and use of a large-sample field-cycled PEDRI imager. *Phys.Med.Biol.* 1998;43:1877-1886.
7. Ardenkjaer-Larsen JH, Laursen I, Leunbach I, Ehnholm G, Wistrand LG, Petersson JS, Golman K. EPR and DNP properties of certain novel single electron contrast agents intended for oximetric imaging. *J.Magn.Reson.* 1998;133:1-12.
8. Alderman DW, Grant DM. An efficient decoupler design which reduces heating in conductive samples in superconducting spectrometers. *J.Magn.Reson.* 1979;36:447-451.
9. Shen GX, Wu JF, Boada FE, Thulborn KR. Experimentally verified, theoretical design of dual-tuned, low-pass birdcage radiofrequency resonators for magnetic resonance imaging and magnetic resonance spectroscopy of human brain at 3.0 Tesla. *Magn.Reson.Med.* 1999;41:268-275.
10. Nestle N, Shet K, Lurie DJ. PEDRI imaging of free radical distribution in environmental science applications – first results and perspectives. MRPM7 proceedings 2004, submitted.

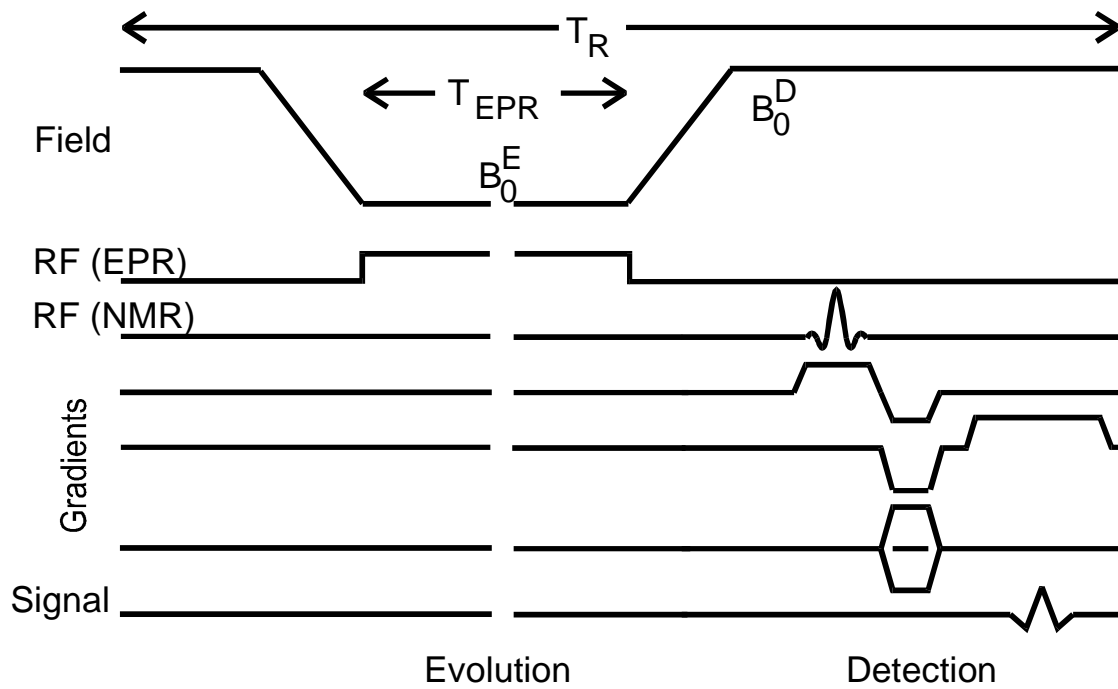


Figure 1

Typical FC-PEDRI pulse sequence, using gradient-echo NMR signal acquisition. In its usual implementation, the pulse sequence is repeated with and without EPR irradiation, in an interleaved fashion, for each line of k-space – i.e. a total of 256 acquisitions are needed for the acquisition of 128×128 pixel images.

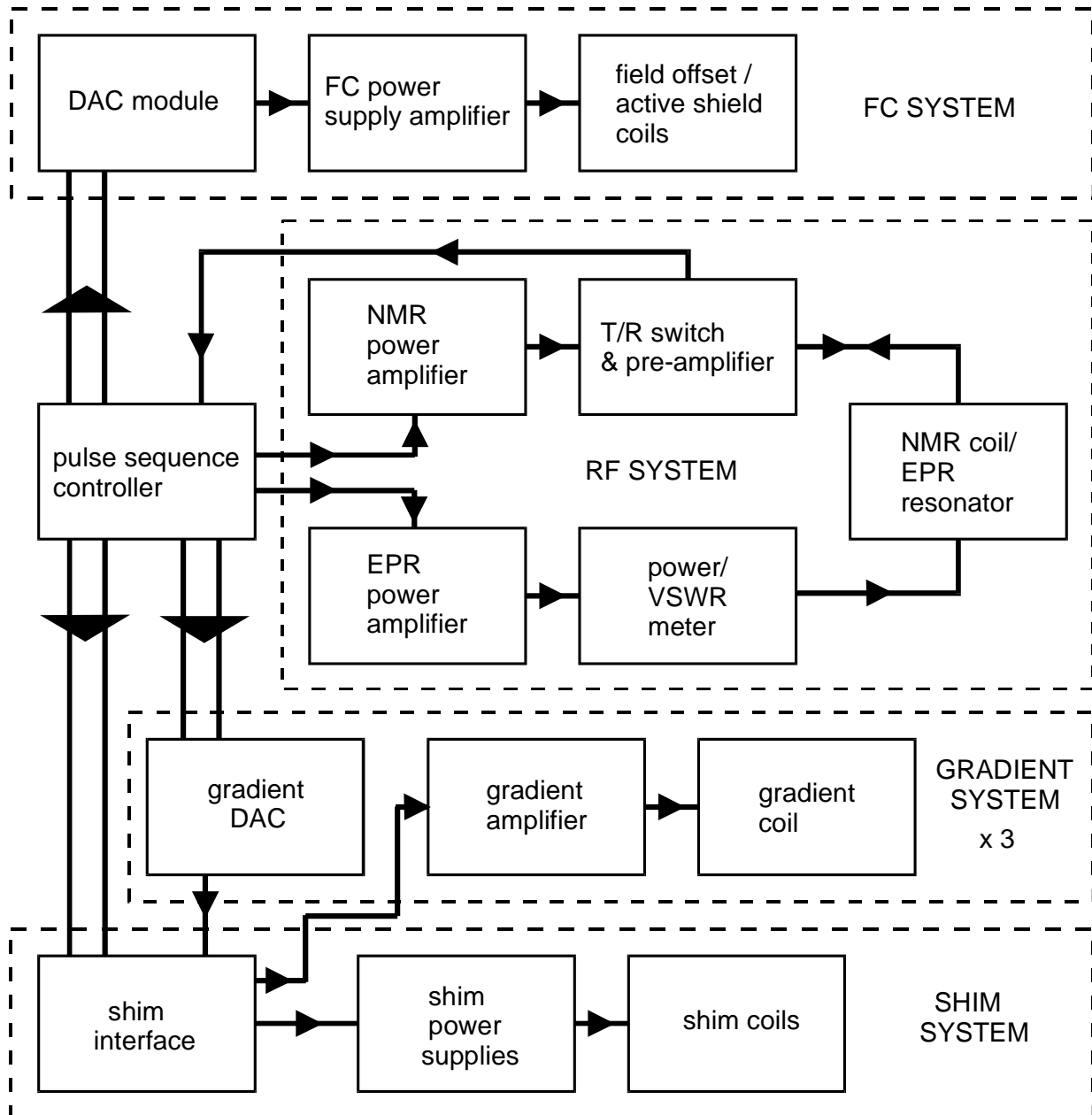


Figure 2. Block diagram of the 450 mT FC-PEDRI system.

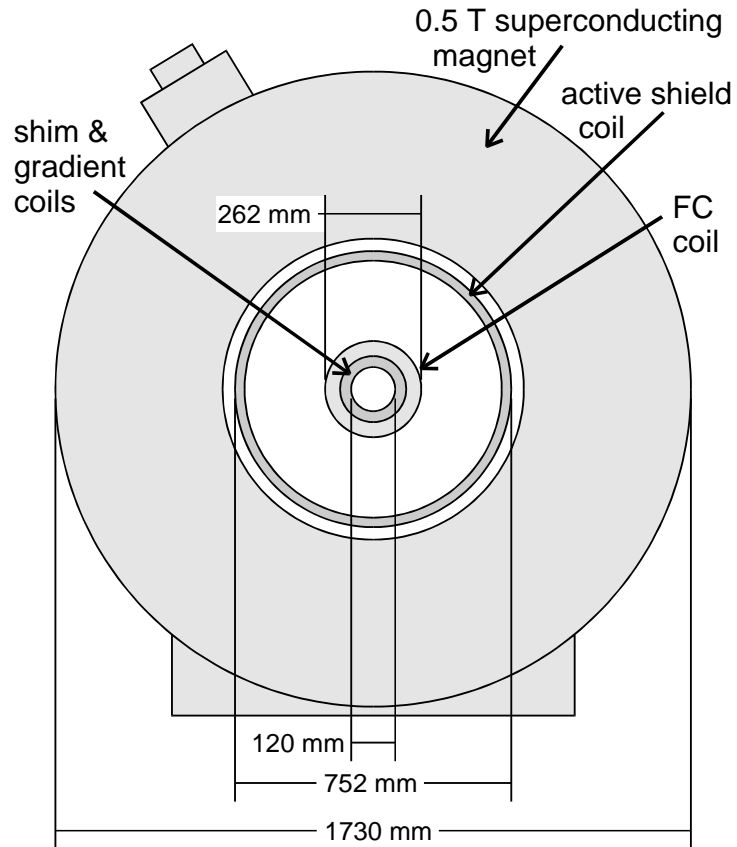


Figure 3.

Schematic diagram showing the components of the field-cycling magnet system, approximately to scale.



Figure 4.

Photograph of the field-cycling magnet system with one of the authors. The tubes entering from the left of the photograph supply cooling water for the field-offset, active-shield and gradient coils; their electrical supply cables enter from the right.

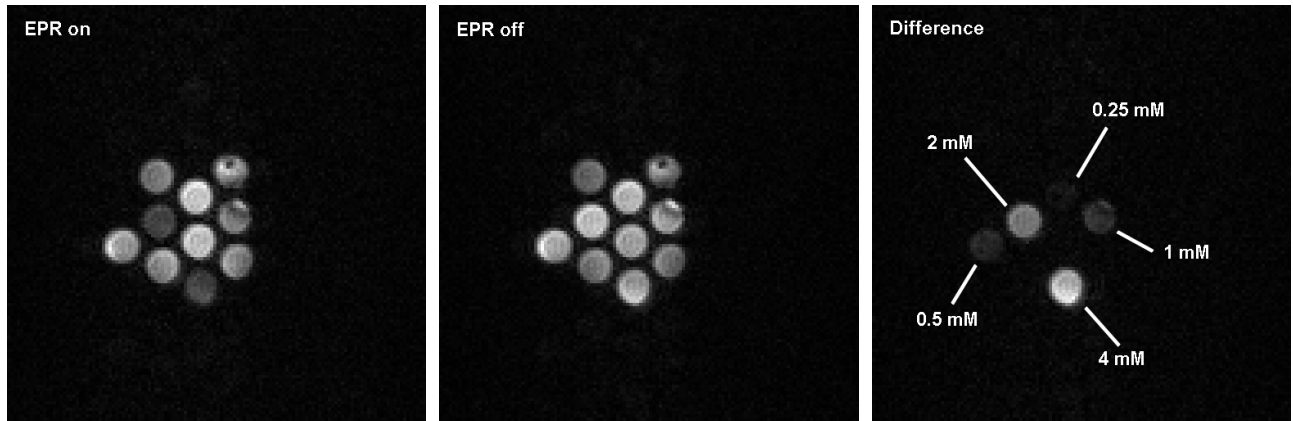


Figure 5 a, b, c

Images of phantom composed of an array of 8 mm internal diameter glass tubes filled with aqueous solutions of TEMPOL nitroxide free radical. Left to right: (a) Image acquired with EPR irradiation; (b) Image acquired without EPR irradiation; (c) Difference image (magnitude of complex difference between with-EPR and without-EPR datasets), labelled with concentrations of visible solutions. Image parameters: 128×128 matrix; FoV 100×100 mm; slice thickness 5 mm; NEX 1; T_R 1800 ms; T_{EPR} 750 ms; B_0^E 4.60 mT; EPR irradiation at 93.6 MHz, 7 W applied power.



Figure 6 a, b, c

Images of 172 gram anesthetized rat, 51 minutes after injection of 0.58 mmol/kg i/v dose of TAM stable free radical. Left to right: (a) Image acquired with EPR irradiation; (b) Image acquired without EPR irradiation; (c) Difference image; labels: RK – right kidney, LK – left kidney, B – bladder.

Acquisition parameters: 128×128 matrix; FoV 100×100 mm; slice thickness 30 mm; NEX 1; T_R 1050 ms; T_{EPR} 400 ms; B_0^E 3.30 mT; EPR irradiation at 93.1 MHz, 15 W applied power.